Assessment of Stage 35 With APNASA

Mark L. Celestina*
NASA Glenn Research Center, Cleveland, Ohio, 44135

and

Richard A. Mulac†
University of Toledo, Cleveland, Ohio, 44135

An assessment of APNASA was conducted at NASA Glenn Research Center under the Fundamental Aeronautics Program to determine their predictive capabilities. The geometry selected for this study was Stage 35 which is a single stage transonic compressor. A speedline at 100% speed was generated and compared to experimental data at 100% speed for two turbulence models. Performance of the stage at 100% speed and profiles of several key aerodynamic parameters are compared to the survey data downstream of the stator in this report. In addition, hub leakage was modeled and compared to solutions without leakage and the available experimental data.

Nomenclature

CKE	=	CMOTT modified k-ε turbulence model
m, MF	=	massflow
P	=	Total Pressure
SKE	=	Standard k-ε turbulence model
T	=	Total Temperature
α	=	absolute flow angle
η	=	adiabatic efficiency
1	=	*Stage inlet station*
2	=	*Measurement reporting station aft of stator*

I. Introduction

IN 1994, a CFD blind test of the predictive capabilities of available turbomachinery codes was conducted by ASME and IGTI. The geometry selected was a transonic fan named Rotor 37 which was tested at NASA Glenn Research Center. A more detailed test was conducted by AGARD in 1998.

There is a current thrust by the NASA Fundamental Aeronautics Program to assess various CFD codes now used by NASA and industry in the analysis of turbomachinery. The goal is to assess the current state of the art of these codes then periodically reassess these codes as advances are made in CFD. As part of this assessment under the Subsonic Fixed Wing project, a single stage compressor, Stage35, designed and tested around 1978 at NASA Glenn Research Center was used to assess the predictive capabilities of APNASA. Performance of the stage at 100% speed and profiles of several key aerodynamic parameters are compared to the survey data downstream of the stator in this report. Two turbulence models as well as results with a hub leakage model are analyzed.

* Aerospace Engineer, Heat Transfer & Turbomachinery Branch, 21000 Brookpark Rd./M.S. 5-9, AIAA Member.
† Senior Research Associate, Heat Transfer & Turbomachinery Branch, 21000 Brookpark Rd./M.S. 5-9, non-AIAA Member.

II. APNASA Code

The analysis code used in the present study solves the Average Passage equation system (see Adamczyk[1] and Adamczyk, Mulac, and Celestina[2]). The equations are discretized using a finite volume formulation and are converged to steady-state with a 4-stage Runge-Kutta scheme employing the standard convergence accelerants such as local time-stepping and implicit residual smoothing. Details of the code can be found in Adamczyk, Celestina, Beach and Barnett[3]. Flow in the clearance gaps was simulated using a model suggested by Kirtley, Beach and Adamczyk[4], which treats the flow through the clearance gap as an orifice flow with no loss in mass, momentum, or energy. The effect of the vena contracta which occurs in orifice flows is accounted for by the use of a discharge coefficient, which sizes the effective tip clearance gap to the actual clearance. A discharge coefficient of 1.0 is used for all results presented herein as advocated by Van Zante, Strazisar, Wood, Hathaway and Okiishi[5]. The turbulence models used in this work were the standard k-ε two equation model and a *CMOTT* modified version of the k-ε two equation model specifically designed for non-equilibrium flows. Details can be found in Shabbir, Zhu and Celestina[6] and Shieh[7].

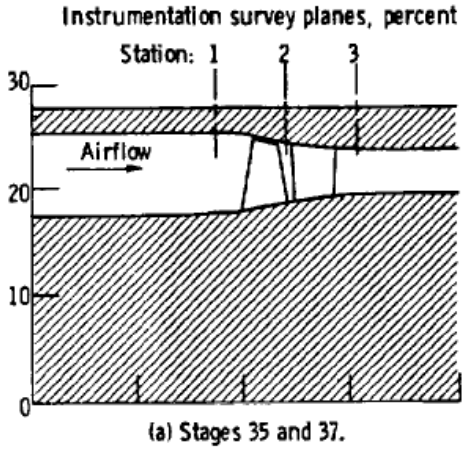

(a) Stages 35 and 37.

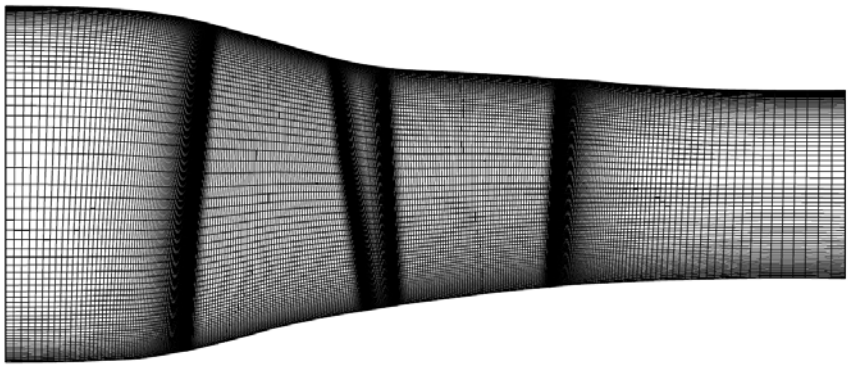

Figure 2. Axisymmetric Mesh for Stage 35.

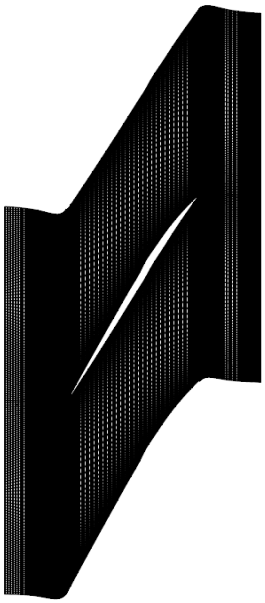

Figure 3. Blade-to-blade view of Rotor 35 tip.

The flowpath of stage 35 is shown in Figure 1 with the instrumentation survey planes. The APNASA solver expects a grid for both rotor and stator of stage 35 with a common axisymmetric grid as shown in Figure 3. The computational grids used for the present calculations were generated using the MMESH turbomachinery grid code developed by Mulac[8]. The grids used by APNASA are sheared H-type in the blade-to-blade direction and incorporate a simple stretching parameter to resolve the boundary layer and adequately define the core flow region. Figure 4 shows a portion of the blade-to-blade rotor mesh near the tip while Figure 5 shows a portion of the blade-to-blade stator mesh near the tip. A stretching parameter is also needed in the span-wise and chord-wise directions to enable adequate resolution of the blade leading and trailing edges and clearance gaps. The blade-to-blade stretching is relaxed to uniform spacing upstream and downstream of the blade rows since the flow is assumed to be periodic in those regions.

The grid for each blade row of stage 35 contained 3.7 million points. Grid sizes for the individual blade rows are given in Table 1. As was mentioned earlier, the tip clearance gaps were modeled. The rotor tip clearance was modeled with four cells across a gap of *.04 cm*. The stator hub clearance gap was modeled with five cells across a gap of *.0762 cm (.03 in*.). The stator was attached to the shroud using a trunnion which was not modeled.

Table 1. Grid Parameters for Stage 35.

Region	Type	Axial Points in Domain	Axial Pts. on Blade Row	Radial Points	Blade-to-Blade Points	Total points
Rotor	H	563	100	81	81	3.7M
Stator	H	563	100	81	81	3.7M

The APNASA system is a process for solving the average-passage flow model. This flow model describes the time average three-dimensional flow field within a passage of a typical blade row embedded within the stage. Each blade row is solved separately with body forces representing its neighboring blade row. Thus, the system is considered converged when the difference between the axisymmetric solutions of both blade rows (axisymmetrically-averaged three-dimensional solutions) are within some prescribed tolerance. Through numerical experiments, it has been found that the body forces need to be updated every fifty iterations on each blade row. This iterative process is known as a swap. Thus, convergence is considered both from a three-dimensional level or blade row level as well as from an axisymmetric level.

The resulting system is highly parallel in a computing environment containing a processor per blade row. For this case, the solutions were generated on a multi-node Linux cluster. For the fine mesh described, each swap for a solution required eight minutes of processing. Thus, a converged solution which required 400 swaps needed 2.2 days of processing on a two node Linux box.

Developing the speedline for stage 35 was a serial process which started with generating a solution at the highest mass flow (choked flow) from an initial guess. This was done by setting a low exit hub static pressure and using radial equilibrium to define the radial static pressure profile. Upon convergence of the choke flow solution, another solution was initiated by setting a higher exit hub static pressure and starting from the previous converged solution at the higher flow rate. The typical number of swaps (body force updates) was set to 400 but was increased to 500 or more as the solutions approached near stall. The number of swaps was set purposely high to insure convergence well beyond what is necessary for results of engineering accuracy. The total pressure, total temperature, radial and tangential flow angles were prescribed at the inlet of the computational domain. The value of these parameters were deduced from the experiment. A boundary layer profile was assumed at the inlet hub and shroud and was based on previous simulations of experiments from this rig.

III. Computed Results

Results for the computationally generated speedline are given in the next figure. The values used in the numerical speedline are computed by integrating the mass-averaged total pressure and total temperature at the inlet station (mesh inlet) surface and the mesh surface downstream of the stator closest to where the experimental data was collected. Predicted choke flow for solutions with either turbulence model was slightly higher (.4%) than the reported experimental value of 20.95 kg/sec. Figure 4(a) shows pressure ratio vs. corrected mass flow for Stage35. The figure presents two speedlines that were generated numerically and are represented with the blue diamond (♦) and green triangle (▲) symbols and compared to the experimental data represented with

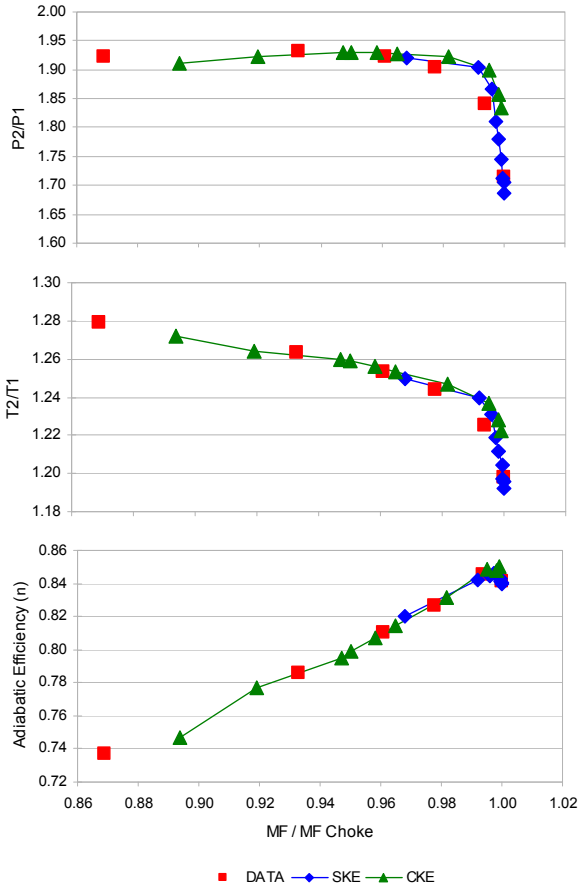

Figure 4. (a) Pressure Ratio, (b) Temperature Ratio, (c) Adiabatic Efficiency vs. Corrected Mass Flow for Stage 35.

the red square (■) symbol. The standard k-ε model (♦ symbol) was not able to generate a converged solution below a corrected mass flow ratio (m/m_{choke}) of 0.974. However, the *CMOTT* k-ε model (▲ symbol) achieved a solution below 0.897 which is near the last stable experimental data point of 0.869. The last two numerical solutions closest to stall exhibited a cyclic behavior in mass flow, pressure ratio and temperature ratio but were carried out far enough (over 1000 swaps) to insure that they did not degenerate into numerical stall. For example, the mass flow for the last stable numerical solution varied by 3% about the mean and ranged from 0.9403 to 0.8878. The temperature ratio (T2/T1) is shown in Figure 4(b) and also agrees well with experiment. The shape of the numerical speedline exhibits the same type of behavior as seen in the pressure ratio. The numerical speedlines in terms of pressure ratio and temperature ratio agree well with the experimental speedline. Figure 4(c) shows the adiabatic efficiency from the numerical speedlines with good agreement to experiment. Both experiment and numerical values of adiabatic efficiency were computed from the total pressure and total temperature values.

Reid and Moore[9] used two combination probes and two wedge probes to survey the flow both radially and circumferentially at a station downstream of the stator to obtain distributions of total pressure, total temperature and flow angle. Comparisons are made at two conditions: high flow which occurs at a mass flow ratio (m/m_{choke}) of 0.9938; and low flow which occurs at a mass flow ratio (m/m_{choke}) of 0.9327. At high flow, Figure 5(a) shows spanwise distributions of total pressure ratio at a station downstream of the stator with comparison to experimental data. The plot compares two numerical solutions with the experimental data at peak efficiency. The simulation solutions shown are for the nearest high flow solution obtained with the standard k-ε turbulence model which corresponds to a pressure ratio of 1.866; and the nearest high flow solution for the *CMOTT* k-ε turbulence model which corresponds to a pressure ratio of 1.899. Table 2 displays the numerical solutions being compared to the experimental data.

Table 2. Comparison of Numerical Solutions to Experimental Data for High Flow.

Type	Symbol	MassFlow (kg/sec)	MassFlow Ratio	P2/P1
Experimental	■	20.82	0.9938	1.842
Standard k-ε	—	20.941	0.9959	1.866
CMOTT k-ε	—	20.924	0.9951	1.899

The numerical solutions at high flow exhibit the same level of total pressure ratio as the experimental data. The hub total pressure deficit in the experimental data is not predicted in the simulations as this may be due to leakage flow which was not modeled here initially. The hub total pressure deficit for a rotor only simulation of this rotor has been reported by Shabbir, Celestina, Adamczyk and Strazisar[10] to be due to leakage flow in a gap between a rotating and

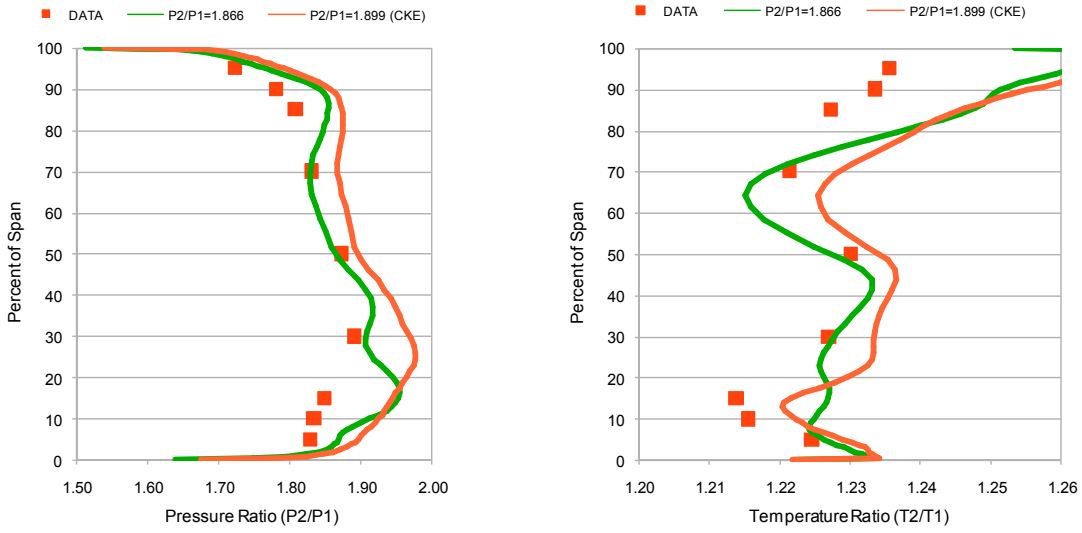

Figure 5. Spanwise Distribution of (a) Pressure Ratio and (b) Temperature Ratio aft of Stator Exit at High Flow.

non-rotating hub component. That paper reports that modeling of the leakage flow is the underlying cause of the hub pressure deficit. The effects of adding a leakage model to the simulation will be shown later in this paper. Comparison of total pressure near the tip shows good agreement. The number of radial cells used to resolve the tip clearance flow is double that used in the ASME / IGTI CFD blind test.

Figure 5(b) shows spanwise distributions of total temperature ratio at the same downstream station of the stator. Comparisons are made of the same numerical simulations that were discussed in Figure 5(a). In general, the spanwise variation of total temperature for the 1.866 and 1.899 pressure ratio solutions show very good agreement through most of the span except near the tip where the experimental data shows a smaller rise in total temperature. The reason for this discrepancy may be due to inadequate rotor tip clearance resolution. This issue was discussed in a paper by Van Zante, Strazisar, Wood, Hathaway, and Okiishi[5] but their recommendations were not completely followed in generating the mesh for this case as this would have led to either a larger radial stretching ratio or increased the number of radial points and thereby increased the necessary computer resources. The experimental data shows a sizable total temperature deficit near the hub which neither solution captures, however, the CMOTT model shows some indication of a deficit. For completeness, the efficiency which is a derived quantity is compared to experimental data in Figure 6(a) for the same numerical solutions. Note that both numerical solutions compare very well with experimental data. Finally for the high flow condition, the flow angle is presented in Figure 6(b) and compared to experimental data. The flow angle distributions from the numerical simulations have the same general shape as the experimental data but underpredict the data by almost five degrees. The cause of this disagreement at high flow is not known but it is reduced by adding a hub leakage model to the simulation.

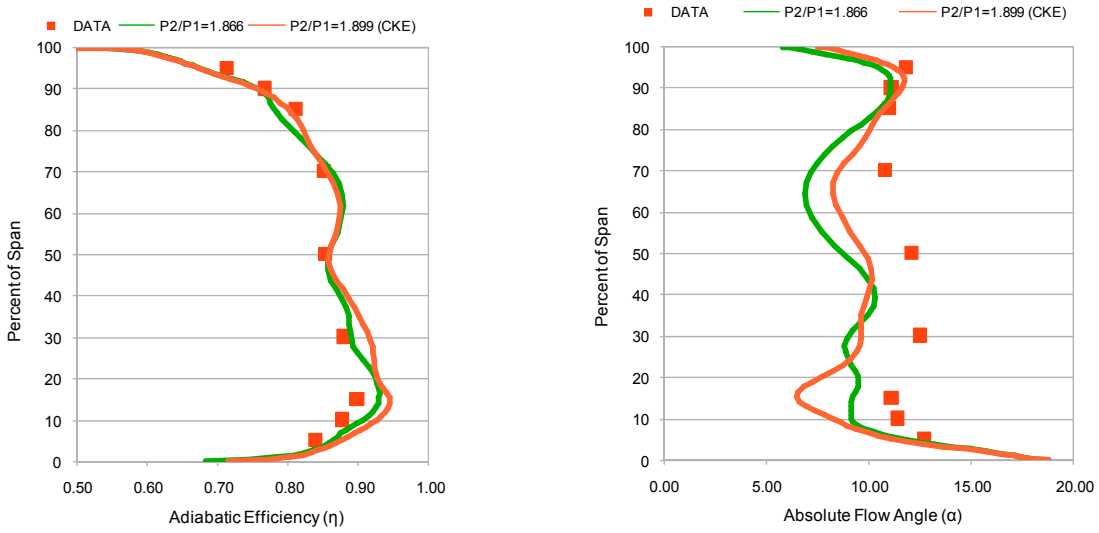

Figure 6. Spanwise distribution of (a) Efficiency and (b) Flow Angle aft of Stator Exit at High Flow.

It was noted earlier that the simulation was nearly able to achieve the lowest experimental mass flow at a mass flow ratio (m/m_{choke}) of 0.87 but the numerical solution exhibited an oscillatory behavior. Thus, the numerical solution at a mass flow ratio (m/m_{choke}) of 0.92 will be compared to the profiles from the low flow experimental data. Figure 7(a) compares the spanwise distribution of total pressure from the numerical solution at a pressure ratio of 1.922 to the experimental data at a pressure ratio of 1.932 at the station aft of the stator. The experimental data shows a hub pressure deficit that developed from the rotor hub platform leakage but is not captured in the numerical profile since this was not modeled in this simulation. However, the remaining spanwise distribution of total pressure from the numerical solution compares very well with experiment. Figure 7(b) shows the comparison of spanwise distribution of total temperature from the same numerical solution and the same experimental data. The data shows a total temperature deficit near the hub which seems to be captured by the numerical simulation. The largest difference between experimental and predicted total temperature occurs at 50% span and translates to about 3°C. For completeness, the adiabatic efficiency is shown in Figure 7(c) for the predicted and experimental data. The comparison is very good near the shroud but shows a slight overprediction from near hub to midspan. However, the shape of the spanwise distribution of efficiency follows the experimental profile. Finally, Figure 7(d) compares the

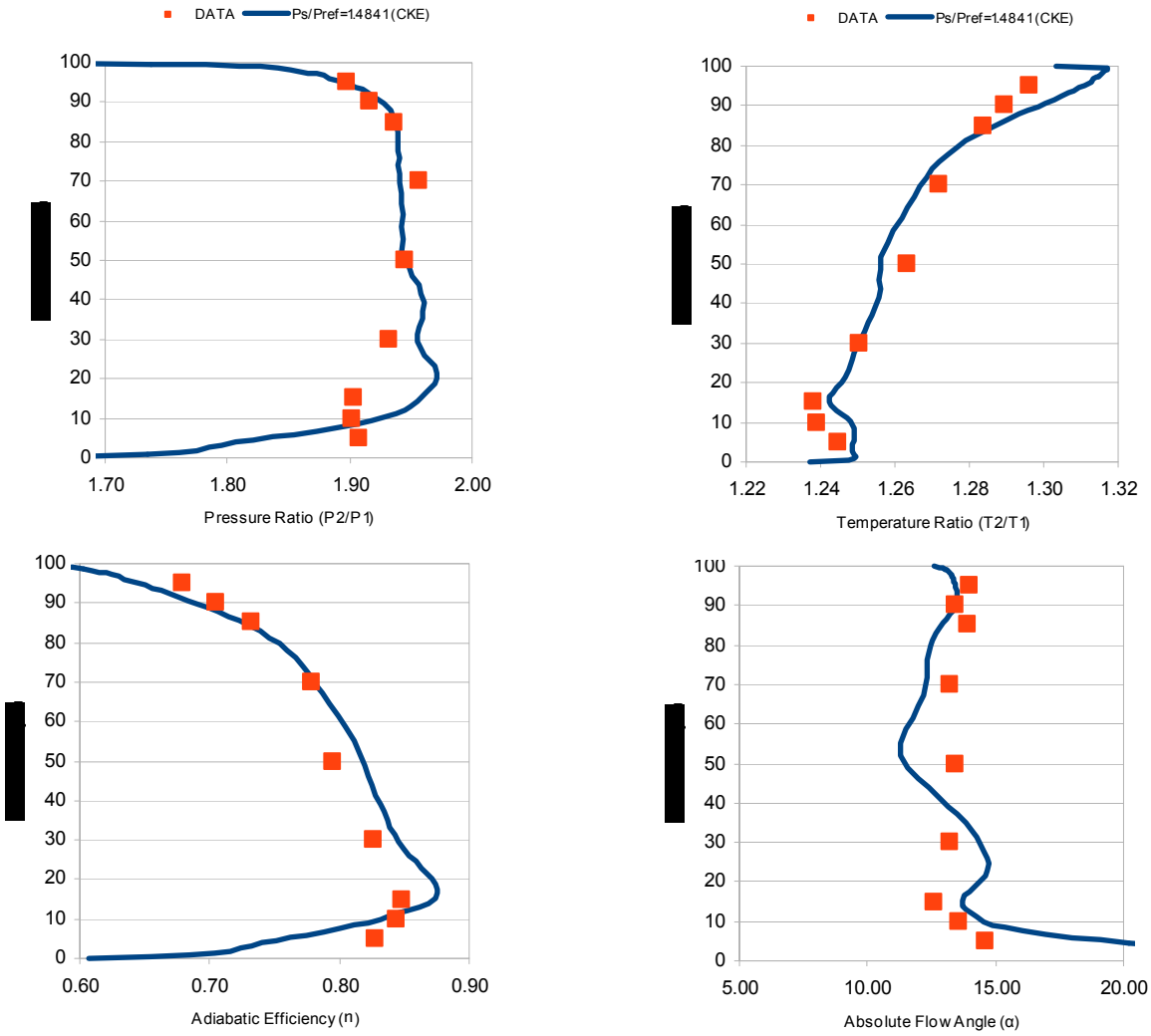

Figure 7. Spanwise Distribution of (a) Pressure Ratio, (b) Temperature Ratio, (c) Adiabatic Efficiency, and (d) Absolute Flow Angle aft of Stator Exit at Low Flow.

flow angles from the predicted solution to the experimental data. The level of underprediction of the flow angle that was shown at peak efficiency is not seen at near stall. The numerical solution shows more variation with radius than the rather flat profile shown in the experimental data outside of the endwall regions.

IV. Hub Leakage Effects

Shabbir, Celestina, Adamczyk, and Strazisar[11] performed a simulation of this rotor and showed that unsteady pumping of a blind under-platform cavity upstream of the rotor by the rotor shock system could impact rotor performance even though there was no net leakage from the cavity. They further showed that this effect could be modeled by introducing a small amount of steady leakage upstream of the rotor hub. Based on this work, rotor hub leakage was modeled by introducing a small amount of flow (.33% of inlet mass flow) into the stream from this region. The effect of adding this small amount of flow to the simulation has a significant effect on the solutions. Seven simulations were carried out with the hub leakage model added at successively increasing back pressures. The resulting speedline is seen in Figure 8 for pressure ratio, temperature ratio and adiabatic efficiency. A comparison is made to the no hub leakage speedline as well as the experimental data. The low flow solution for the hub leakage model was generated with a fixed exit corrected mass flow boundary condition. This boundary

condition was developed by Adamczyk[‡]. The simulation with this boundary condition converges to a fixed corrected flow in less iterations than the radial equilibrium boundary condition at lower flows. No attempt was made to obtain the lowest stable solution with the hub leakage model.

Modeling the hub leakage resulted in a numerical speedline that compared very well with the experimental speedline. Note that the distinctive bend in the pressure ratio without the hub leakage modeled is not seen in the speedline with the hub leakage model. In the model, the leakage at the hub is injected into the flow. Shabbir, Celestina, Adamczyk, and Strazisar[11] reported that this type of hub leakage reduces the pressure rise capability of the rotor. In addition, that paper reported that hub leakage resulted in the formation of a near-hub deficit in total pressure in addition to causing a reduction in pressure rise over the entire span. This finding is also evident here and is seen in Figure 9. The hub leakage solution is compared to the numerical solution without hub leakage and the experimental data at high flow for total pressure and total temperature ratio. The addition of the hub leakage gives a much better comparison to the experimental data in overall level as well as near the hub and near the tip in total pressure. The total temperature profile with hub leakage clearly shows the deficit seen in the experimental data. For completeness, Figure 10(a) shows the adiabatic efficiency for the two numerical solutions compared to the experimental

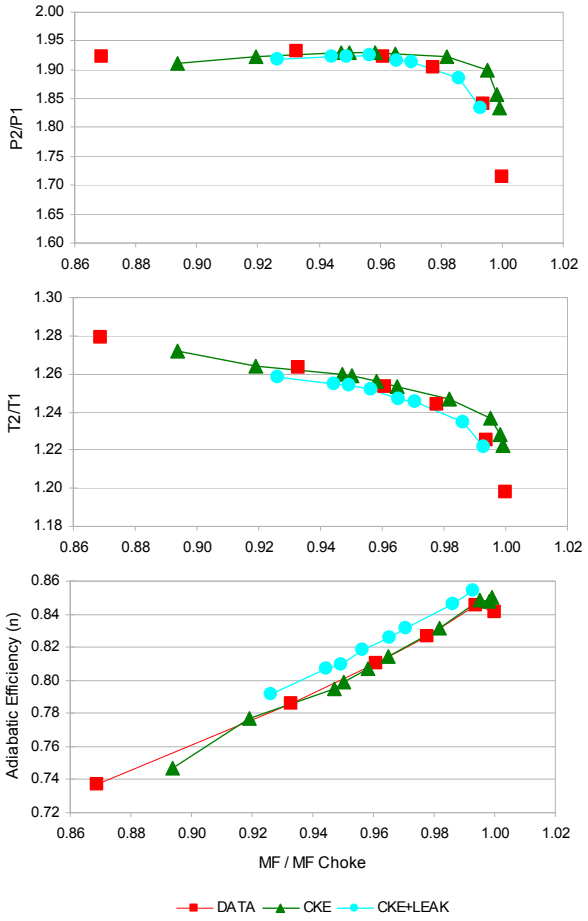

Figure 8. (a) Pressure Ratio, (b) Temperature Ratio, and (c) Adiabatic Efficiency vs. Corrected Mass Flow Ratio for Hub Leakage Model.

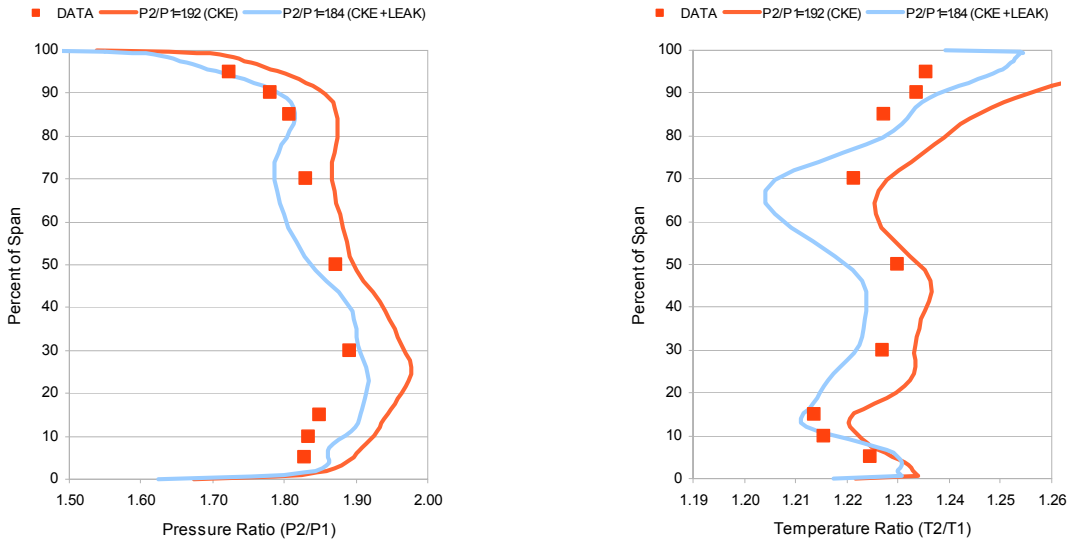

Figure 9. Spanwise Distribution of (a) Total Pressure Ratio and (b) Total Temperature Ratio aft of Stator Exit at High Flow with Hub Leakage.

[‡] Private Communication.

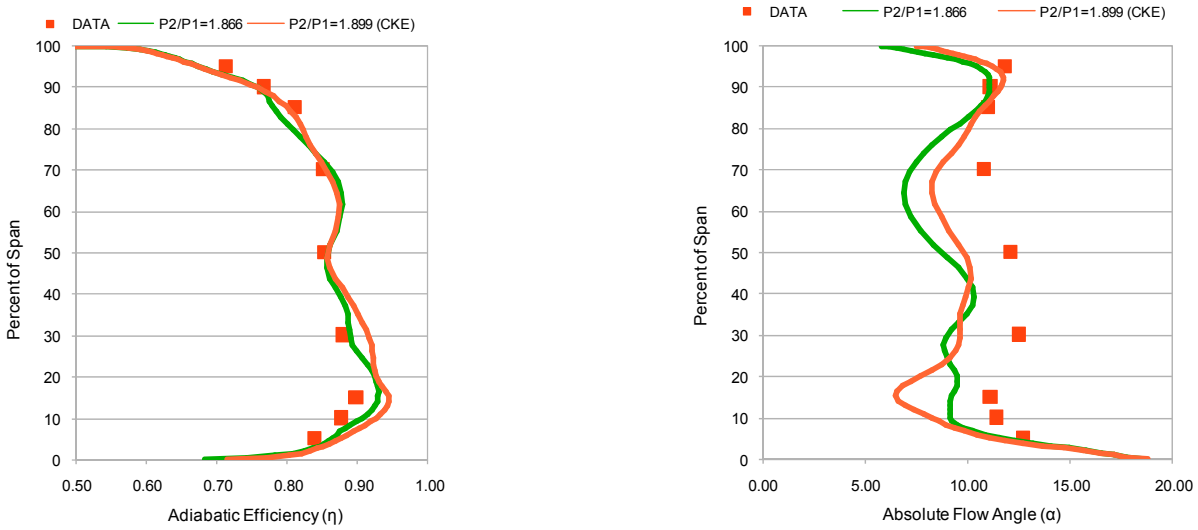

Figure 10. Spanwise distribution of (a) Adiabatic Efficiency and (b) Absolute Flow Angle aft of Stator Exit at High Flow with Hub Leakage.

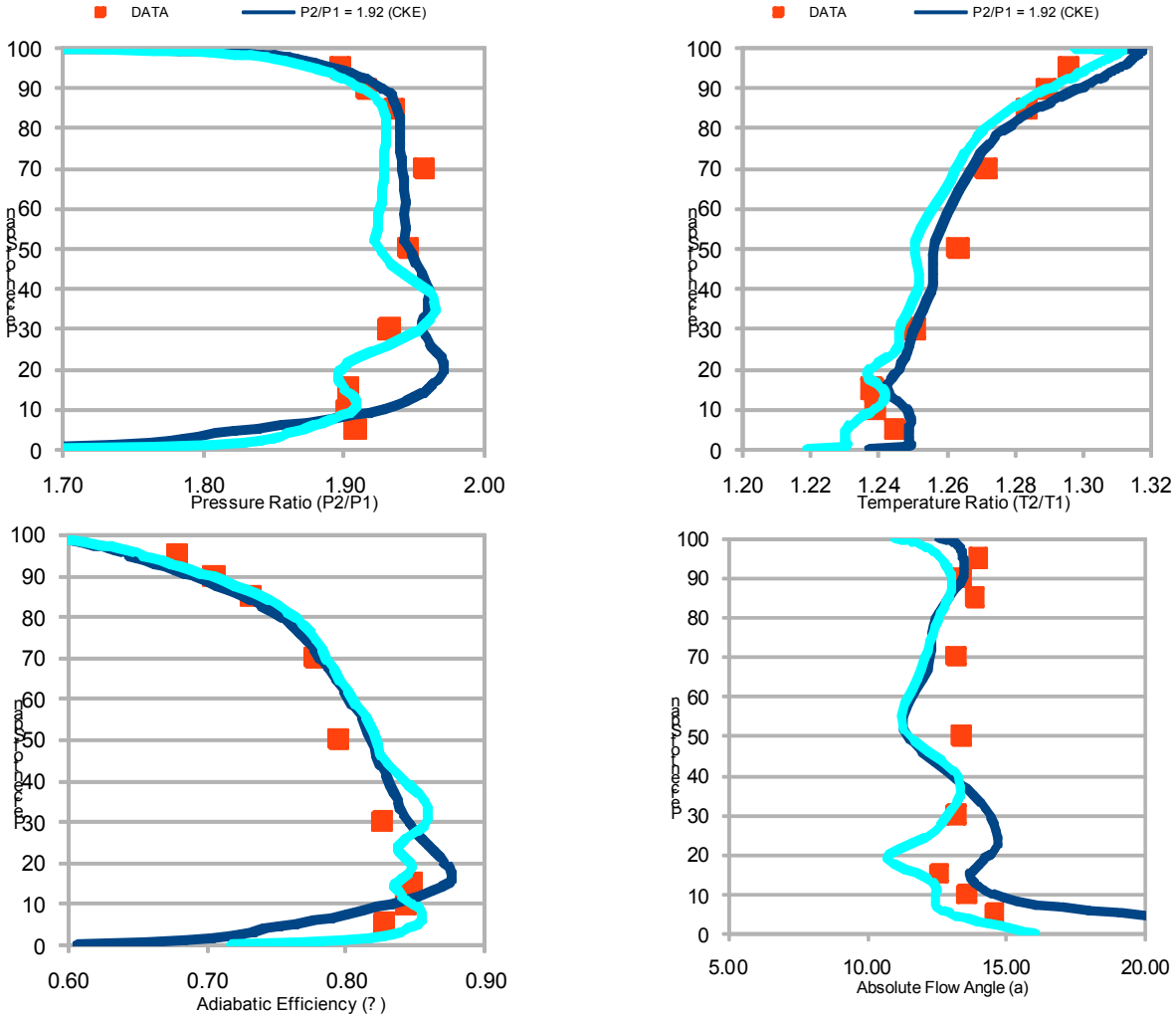

Figure 11. Spanwise distribution of (a) Total Pressure Ratio, (b) Total Temperature Ratio, (c) Adiabatic Efficiency, and (d) Absolute Flow Angle aft of Stator Exit at Low Flow with Hub Leakage.

data. The absolute flow angle comparison is given in Figure 10(b). Note the better agreement of the flow angles to the experimental data near the hub. However, the midspan region actually shows more disagreement with the leakage model in comparison to the data. Figure 11 shows the spanwise distribution of Total Pressure Ratio, Total Temperature Ratio, Adiabatic Efficiency and Absolute flow angle at low flow for the solution with the hub leakage model compared to the experimental data and the solution without the hub leakage model. The total pressure deficit in the hub compares well with experiment in Figure 11(a). In Figure 11(b), the temperature deficit occurs at a higher span than the experiment but the total temperature near the tip agrees quite well. In Figure 11(c), the flow angle from the leakage model solution shows good agreement with experiment near the hub at low flow. Thus, the leakage model overall compares better to the experimental data than the solutions with no leakage model at the hub.

V. Conclusion

APNASA, an analysis code developed by NASA for multistage turbomachinery was used to simulate Stage35, a NASA designed and tested transonic compressor stage. The objective was to generate and compare a speedline of Stage35 at 100% design speed with experimental data and compare spanwise profiles at two points, high flow and low flow, on the speedline. APNASA used two turbulence models for the comparison, the standard k-ε model and the *CMOTT* k-ε model. The *CMOTT* k-ε model was developed for flows that are not in local equilibrium. The predicted speedline for both turbulence models agreed well with the experimental data, however, the *CMOTT* k-ε model was able to predict the flow to near stall. In terms of spanwise distributions of total pressure, total temperature, adiabatic efficiency and flow angle, the *CMOTT* k-ε model overall agreed better with the experimental data. Because of the known cavity between the rotating and stationary hub upstream of the rotor, a hub leakage model was added to the simulation. The inclusion of this hub leakage model upstream of the rotor showed much better agreement to the experimental data both in the speedline as well as in the profiles. This was clearly evident in the profiles of total temperature and pressure especially in the hub region. An area identified in the numerical simulations that did not predict well with experimental data was the flow angle underprediction of almost 5 degrees at high flow. The reason for this difference is not known and would be difficult to investigate further since the experimental data for this stage is not available in an unprocessed form and the hardware does not exist anymore.

Acknowledgments

The preferred spelling of the word “acknowledgment” in American English is without the “e” after the “g.” Avoid expressions such as “One of us (S.B.A.) would like to thank…” Instead, write “F. A. Author thanks…” *Sponsor and financial support acknowledgments are also to be listed in the “acknowledgments” section.*

References

[1] Adamczyk, J.J., 1984, “Model Equation for Simulating Flows in Multistage Turbomachinery,” ASME Paper 85-GT-226. (NASA TM-86869).

[2] Adamczyk, J.J., Mulac, R.A., and Celestina, M.L., 1986, “A Model for Closing the Inviscid Form of the Average Passage Equation System,” ASME Paper 86-GT-227. (NASA TM-87199).

[3] Adamczyk, J.J., Celestina, M.L., Beach, T.A., and Barnett, M., “Simulation of 3-D Viscous Flow within a Multi-stage Turbomachine,” TM 101376, 1989.

[4] Kirtley, K. R., Beach, T. A., and Adamczyk, J. J., “Numerical Analysis of Secondary Flow in a Two-Stage Turbine,” Paper No. AIAA-90-2356, 1990.

[5] Van Zante, D., Strazisar, A., Wood, J., Hathaway, M., Okiishi, T., “Recommendations for Achieving Accurate Numerical Simulation of Tip Clearance Flows in Transonic Compressor Rotors,” J of Turbomachinery, Vol 122, P. 733, October 2000.

[6] Shabbir, A., Zhu, J., and Celestina, M., “Assessment of Three Turbulence Models in a Compressor Rotor,” ASME 96-GT-198, June 1996.

[7] Shieh, T.-H., “Some Developments In Computational Modeling of Turbulent Tlows,” Fluid Dynamics Research

20, pp. 67-96, 1997.

[8] Mulac, R.A., "A Multistage Mesh Generator for Solving the Average-Passage Equation System," NASA CR-179539, January 1988.

[9] Reid, L. and Moore, R., "Performance of Single-Stage Axial-Flow Transonic Compressor With Rotor and Stator Aspect Ratios of 1.19 and 1.26, Respectively, and With Design Pressure Ratio of 1.82" NASA TP 1338, November 1978.

[10] Shabbir, A., Celestina, M. L., Adamczyk, J. J., and Strazisar, A. J., "The Effect of Hub Leakage Flow on Two High Speed Axial Compressor Rotors," ASME Paper 97-GT-346, June 1997.

[11] Shabbir, A., Celestina, M. L., Adamczyk, J. J., and Strazisar, A. J., "The Effect of Hub Leakage Flow on Two High Speed Axial Compressor Rotors," ASME Paper 97-GT-346, June 1997.